

Long-period radio pulsars: population study in the neutron star and white dwarf rotating dipole scenarios

N. REA,^{1,2} N. HURLEY-WALKER,³ C. PARDO-ARAUJO,^{1,2} M. RONCHI,^{1,2} V. GRABER,^{1,2} F. COTI ZELATI,^{1,2}
D. DE MARTINO,⁴ A. BAHRAMIAN,³ S. J. MCSWEENEY,³ T. J. GALVIN,^{5,3} S. D. HYMAN,⁶ AND M. DALL'ORA⁴

¹*Institute of Space Sciences (ICE), CSIC, Campus UAB, Carrer de Can Magrans s/n, E-08193, Barcelona, Spain*

²*Institut d'Estudis Espacials de Catalunya (IEEC), Carrer Gran Capità 2-4, E-08034 Barcelona, Spain*

³*International Centre for Radio Astronomy Research, Curtin University, Kent St, Bentley WA 6102, Australia*

⁴*INAF – Capodimonte Astronomical Observatory Naples Via Moiariello 16, I-80131 Naples, Italy*

⁵*CSIRO, Space and Astronomy, PO Box 1130, Bentley WA 6102, Australia*

⁶*Department of Engineering and Physics, Sweet Briar College, Sweet Briar, VA 24595, USA*

(Received July, 2023)

Submitted to ApJ

ABSTRACT

The nature of two recently discovered radio emitters with unusually long periods of 18 min (GLEAM-X J1627–52) and 21 min (GPM J1839–10) is highly debated. Their bright radio emission resembles that of radio magnetars, but their long periodicities and lack of detection at other wavelengths challenge the neutron-star interpretation. In contrast, long rotational periods are common in white dwarfs but, although predicted, dipolar radio emission from isolated magnetic white dwarfs has never been unambiguously observed. In this work, we investigate these long-period objects as potential isolated neutron-star or white-dwarf dipolar radio emitters and find that both scenarios pose significant challenges to our understanding of radio emission via pair production in dipolar magnetospheres. We also perform population-synthesis simulations based on dipolar spin-down in both pictures, assuming different initial-period distributions, masses, radii, beaming fractions, and magnetic-field prescriptions, to assess their impact on the ultra-long pulsar population. In the neutron-star scenario, we do not expect a large number of ultra-long period pulsars under any physically motivated (or even extreme) assumptions for the period evolution. On the other hand, in the white-dwarf scenario, we can easily accommodate a large population of long-period radio emitters. However, no mechanism can easily explain the production of such bright coherent radio emission in either scenarios.

Keywords: stars: neutron — pulsars: general — stars: individual (GPM J1839–10, GLEAM-X J1627–52)

1. INTRODUCTION

Highly polarized and periodic Galactic radio sources have been historically interpreted as rotating magnetic neutron-star (NS) dipoles. Until recently, measured periods clustered between about 1 ms – 20 s in line with predictions of recycling scenarios (Bhattacharya & van den Heuvel 1991; Tauris 2012) for the fast and magnetic-field decay (Viganò et al. 2013a; Pons et al. 2013) for the slow rotators. The discovery of ultra-long periodic coherent radio emitters challenges

these models. Some seem to be extreme NS pulsars (e.g., the 76-s source PSR J0901–4046; Caleb et al. 2022), while the interpretation of others is still uncertain (e.g., the 18-minute source GLEAM-X J1627–52; Hurley-Walker et al. 2022). The periodic radio emission of GLEAM-X J1627–52 lasted only a few months in 2018 with a flux density (20-50 Jy) and polarization degree (~90% linear) similar to other radio magnetars, and its long periodicity can be explained through post-supernova fallback accretion (see, e.g., Alpar et al. 2001; Chatterjee et al. 2000; Ertan et al. 2009; Tong et al. 2016; Ronchi et al. 2022). However, deep X-ray limits challenge the magnetar interpretation (Rea et al. 2022).

In contrast, slow spin periods are common in magnetic white dwarfs (MWDs) (Ferrario & Wickramasinghe 2005; Ferrario et al. 2020). Although isolated MWDs exhibit magnetic-field strengths between 10^6 to 10^9 G (Ferrario et al. 2015, 2020), lower than NS B -fields spanning 10^8 to 10^{15} G, MWD have also been proposed to emit spin-down-driven radio emission similar to NSs (Zhang & Gil 2005). To date, two radio-emitting WDs have been detected, the binary systems AR Sco ($P \sim 1.95$ min in a 3.5 hr orbit; Marsh et al. 2016) and J1912–4410 ($P \sim 5.3$ min in a 4 hr orbit; Pelisoli et al. 2023). The radio emission of both systems is partly compatible with dipolar spin-down (Geng et al. 2016; Buckley et al. 2017; du Plessis et al. 2019), but also has a significant component resulting from the intrabinary shock with the wind of the companion star. The lack of an optical/infrared counterpart to GLEAM-X J1627–52 at the estimated distance of 1.3 kpc rules out a similar binary system for this source (Rea et al. 2022). However, it does not exclude lower mass companions, or the possibility of a relatively cold isolated MWD.

We recently discovered another ultra-long period radio pulsar, GPM J1839–10, which has been active continuously for > 33 years (Hurley-Walker et al. 2023). GPM J1839–10 has a periodicity of ~ 21 minutes, estimated distance of ~ 5.7 kpc and radio luminosity of 10^{27-28} erg s $^{-1}$ (peak fluxes of $\sim 0.1 - 10$ Jy). Its long-duration activity allowed us to infer a stringent constraint on its period derivative of 3.6×10^{-13} s s $^{-1}$, resulting in strong limits on its B -field of $< 1.9 \times 10^{15}$ G and rotational power $\dot{E} < 2.1 \times 10^{25}$ erg s $^{-1}$, about 2-3 orders of magnitudes lower than its detected radio luminosity.

In the following, we study GLEAM-X J1627–52 and GPM J1839–10 in the context of the radio emission expected from spin-down of an isolated NS and WD by means of death-line analyses (Sec. 2) and population-synthesis simulations (Sec. 3).

2. DEATH VALLEYS FOR NEUTRON-STAR AND WHITE-DWARF RADIO PULSARS

Radio emission from rotating magnetospheres is usually explained as a result of pair production just above the polar caps (Ruderman & Sutherland 1975). However, for certain limiting periods, magnetic-field strengths and geometries, radio pulsars can no longer produce pairs, and radio emission ceases.

The parameter space in the $P - B$ plane (or equivalently $P - \dot{P}$ plane) below which radio emission is quenched is called the “death valley” (Chen & Ruderman 1993; Zhang et al. 2000). This death valley encompasses a large variety of death lines depending on the

magnetic-field configuration (e.g., dipolar, multi-polar, twisted), the nature of the seed gamma-ray photons for pair production (i.e., curvature or inverse Compton photons), the pulsar obliquity, the stellar radius and moment of inertia (see Suvorov & Melatos 2023 for a death-valley discussion for long-period pulsars). These death-line models have been applied exclusively to NS pulsars because, until very recently, no WD pulsed radio emission had been detected. However, MWDs might not be unlike NS pulsars in generating coherent radio emission through magnetospheric spin-down losses (Zhang & Gil 2005), albeit with different stellar radii, masses and magnetic fields.

Figure 1 shows death valleys for NS and WD pulsars as red and blue shaded regions, respectively. Their boundaries are marked by two death-line extremes (Chen & Ruderman 1993), representing the broadest range of B -field configurations:¹

- a pure dipole with

$$B \simeq 2.2 \times 10^{12} \text{ G } R_6^{-19/8} \left(\frac{P}{1 \text{ s}} \right)^{15/8}; \quad (1)$$

- an extremely twisted, multipolar magnetic field located in a small spot above the polar cap with

$$B \simeq 9.2 \times 10^{10} \text{ G } \chi^{-1/4} R_6^{-2} \left(\frac{P}{1 \text{ s}} \right)^{3/2}, \quad (2)$$

where $R_6 = R/10^6$ cm, and χ is the ratio between the spot’s B -field and the dipolar strength (we assume an extreme value of $\chi = 10$).

For Fig. 1, we use a fiducial NS radius of $R_{\text{NS}} = 11$ km. For WDs, we assume $R_{\text{WD}} = 6000$ km consistent with the Hamada-Salpeter relation (Hamada & Salpeter 1961) and measurements of isolated MWDs (Ferrario et al. 2015, 2020).

For observed NS pulsars, we derive surface magnetic fields at their poles using P and \dot{P} measurements, employing the classical dipolar loss formula $B = (3c^3 I P \dot{P} / 2\pi^2 R^6)^{1/2} \simeq 6.4 \times 10^{19} \sqrt{\dot{P} P} \text{ G}$, (assuming $M_{\text{NS}} = 1.4 M_{\odot}$). B -fields at the poles of isolated WDs are obtained from observations (i.e., Zeeman splitting of spectral lines; Ferrario et al. 2015, 2020; Caiazzo et al. 2021). For the radio pulsating WDs AR Sco and

¹ We note that although these death lines rely on simplifications compared to more recent works (e.g., Zhang et al. 2000), our focus is on the extremes of the death valley. All newer models incorporating more detailed physics fall within the shaded region for any reasonable NS or WD parameters.

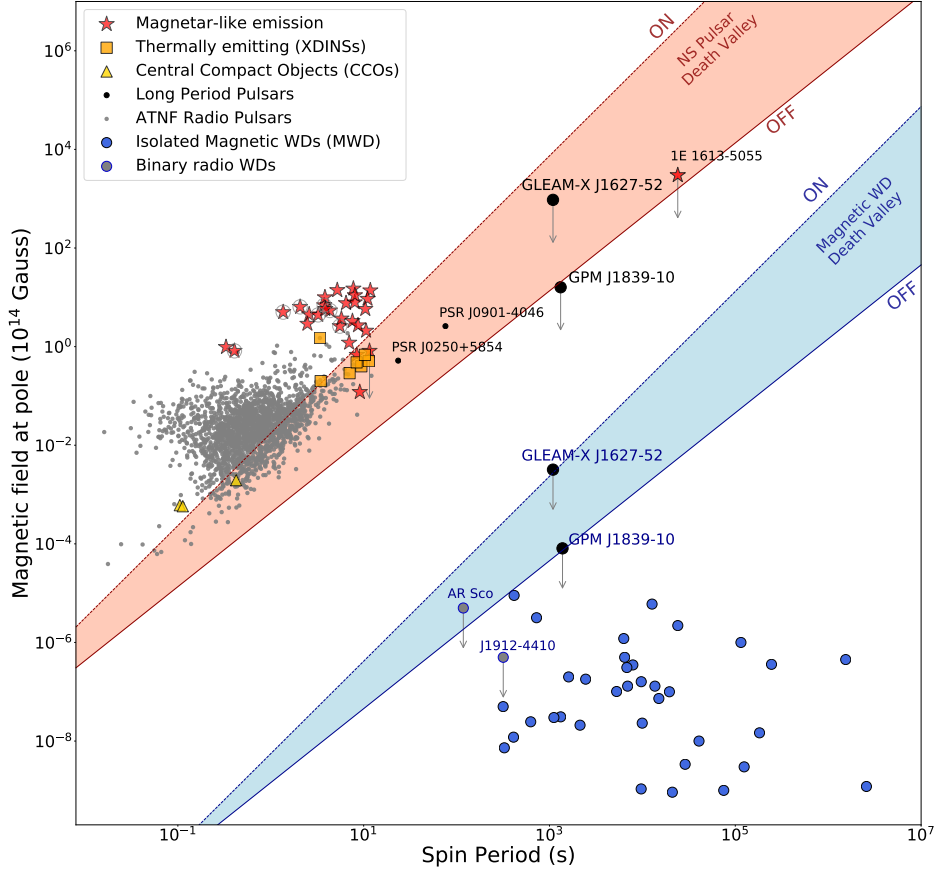


Figure 1. Surface dipolar magnetic field, B , against spin period, P , for observed isolated NSs and magnetic WDs. GPM J1839–10 and GLEAM-X J1627–52 are interpreted as isolated NSs or WDs. Arrows represent upper B -field limits. We show isolated ATNF radio pulsars (Manchester et al. 2005a) (gray dots), pulsars with magnetar-like X-ray emission (red stars; gray circles highlight the radio magnetars), including the long-period magnetar 1E 161348-5055 (De Luca et al. 2006; Rea et al. 2016; D’Ai et al. 2016), X-ray Dim Isolated NSs (XDINSs; orange squares) and Central Compact Objects (CCOs; gold triangles) (Olausen & Kaspi 2014; Coti Zelati et al. 2018). Other long-period radio pulsars are reported as black circles (Tan et al. 2018; Caleb et al. 2022). Isolated MWDs are represented by blue dots (Ferrario et al. 2020; Caiazzo et al. 2021; Buckley et al. 2017). Gray dots show upper B -field limits for the binary WDs AR Sco (Buckley et al. 2017) and J1912-4410 (Pelisoli et al. 2023, 2024). Dashed (solid) lines correspond to theoretical death lines for a pure dipole (extremely twisted multipole) configuration. Red and blue shaded regions indicate NS and WD death valleys, respectively.

J1912–4410, we estimate upper B -field limits assuming the emission to result from dipolar losses (Buckley et al. 2017). Finally, we also show the upper limits on the surface dipolar B -fields of the two long-period radio sources GLEAM-X J1627–52 and GPM J1839–10.

3. POPULATION SYNTHESIS FOR NEUTRON-STAR AND WHITE-DWARF RADIO PULSARS

We simulate isolated NS and WD populations using the framework of Graber et al. (in prep; see also Ronchi et al. (2021)) with model parameters adjusted for each object type. Initially, we randomly sample the logarithm of the birth periods and magnetic fields from normal distributions, and the inclination angle between the magnetic and the rotational axis from a uniform distribution in spherical coordinates. Assuming that NSs and WDs spin down due to magnetospheric torques, we then evolve their periods, P , and inclination angles, χ ,

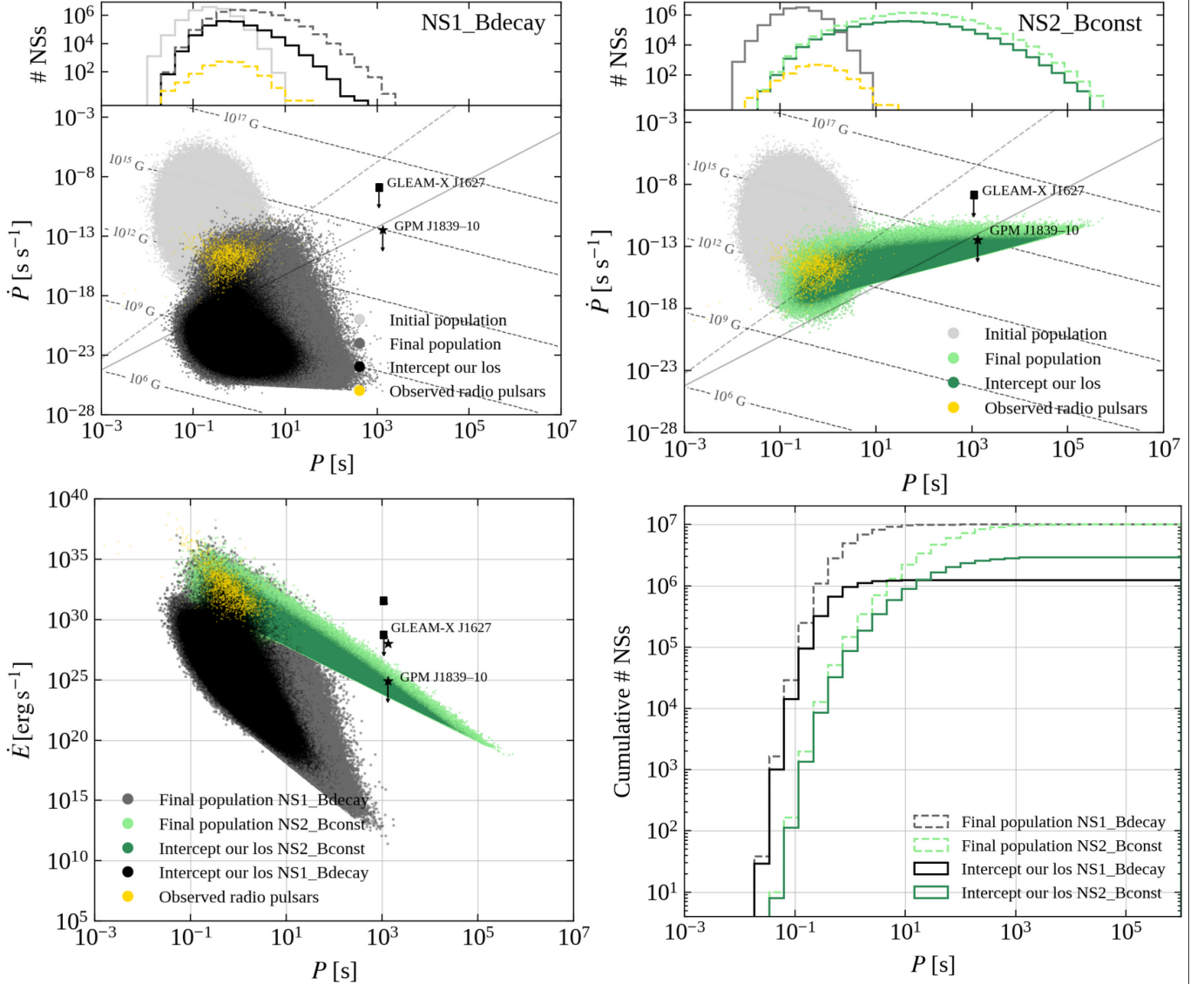


Figure 2. Population-synthesis results for models NS1_Bdecay (black) and NS2_Bconst (green). Top panels show $P - \dot{P}$ diagrams for both simulations, respectively. Light gray dots represent initial NS populations, dark gray and light green final populations. The subsets of objects intercepting our line of sight (l.o.s) are shown in black and dark green. Yellow dots are the observed isolated pulsar population from the ATNF Pulsar Catalogue (Manchester et al. 2005b). Dotted lines of constant B -field are indicated for reference as well as the limits of the death valley and the upper limits for GLEAM-X J1627–52 (square) and GPM J1839–10 (star) as in Fig. 1. Histograms above the $P - \dot{P}$ diagrams represent the corresponding period distributions. The bottom left panel shows \dot{E} versus P for the evolved populations, where we highlight the radio luminosity (top markers) and upper limits on \dot{E} (bottom arrows) for the two sources. The bottom right panel highlights the cumulative period distributions.

over time by solving the coupled differential equations (Philippov et al. 2014; Spitkovsky 2006)

$$\dot{P} = \frac{\pi^2 B^2 R^6}{c^3 IP} (\kappa_0 + \kappa_1 \sin^2 \chi), \quad (3)$$

$$\dot{\chi} = -\frac{\pi^2 B^2 R^6}{c^3 IP^2} (\kappa_2 \sin \chi \cos \chi), \quad (4)$$

where we assume for simplicity $I = 2/5MR^2$ and $\kappa_0 \simeq \kappa_1 \simeq \kappa_2 \simeq 1$ for pulsars surrounded by magnetospheres. Finally, we determine the number of stars that point

towards the Earth by assuming a random direction for the line of sight and employing a prescription for the aperture of the radio beam.

To compare the impact of various initial model assumptions on the final spin-period distributions, we carry out the population simulations summarized in Tab. 1 and Figs. 2–4. Specifically, in Tab. 1, to help the reader, we count the objects falling within the period ranges $10 - 10^2$ s, $10^2 - 10^3$ s, and $10^3 - 10^5$ s. We then distinguish objects intercepting our lines of

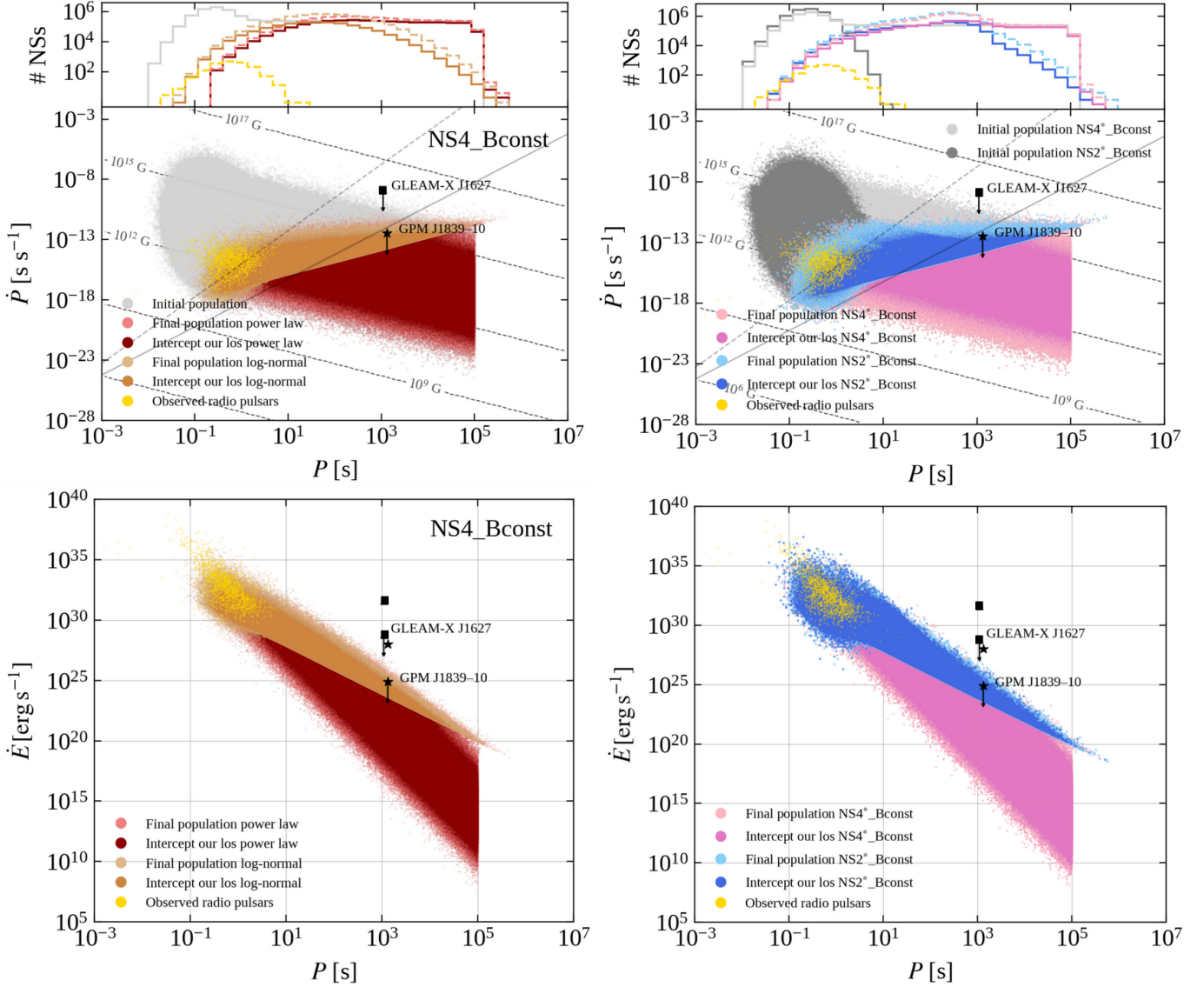


Figure 3. Population-synthesis results for models NS4_Bconst (orange/red), NS2*_Bconst (blue), and NS4*_Bconst (pink). Panels, lines, markers and yellow dots are similar to Fig. 2. In both left panels, evolved objects sampled from the log-normal (power-law) contribution to the initial period distribution are shown in orange (red). Right panels show evolved population of models NS4*_Bconst and NS2*_Bconst based on a bimodal B-field distributions. Across all panels, light shades depict evolved populations, while objects intercepting our lines of sight are shown in dark shades.

sight and those with $\dot{E} > 10^{27} \text{ erg s}^{-1}$ (see Figs. 2–4 for the exact \dot{E} and P distributions). The latter limit has no intrinsic meaning, but was chosen as a reference to show how many sources would have sufficient rotational power to support GPM J1839–10’s radio luminosity. In Figs. 2–4, we also report in the $P - \dot{P}$ plane the two death-line extremes defined in Sec. 2. This is done by making explicit the dependence on the stellar mass and radius and substituting $B = (3c^3 I P \dot{P} / 2\pi^2 R^6)^{1/2} \simeq 5.7 \times 10^{19} (M/M_\odot)^{1/2} R_6^{-2} \sqrt{\dot{P} P} G$ into Eqs. (1) and (2).

In this way we obtain:

$$\dot{P} \simeq 1.5 \times 10^{-15} \text{ s s}^{-1} \left(\frac{M}{M_\odot} \right)^{-1} R_6^{-3/4} \left(\frac{P}{1 \text{ s}} \right)^{11/4}; \quad (5)$$

$$\dot{P} \simeq 2.6 \times 10^{-18} \text{ s s}^{-1} \chi^{-1/2} \left(\frac{M}{M_\odot} \right)^{-1} \left(\frac{P}{1 \text{ s}} \right)^2; \quad (6)$$

for a pure dipole or an extremely twisted multipolar field, respectively. Note that the second death line only depends on the NS or WD mass but not on their radius.

3.1. NS population synthesis

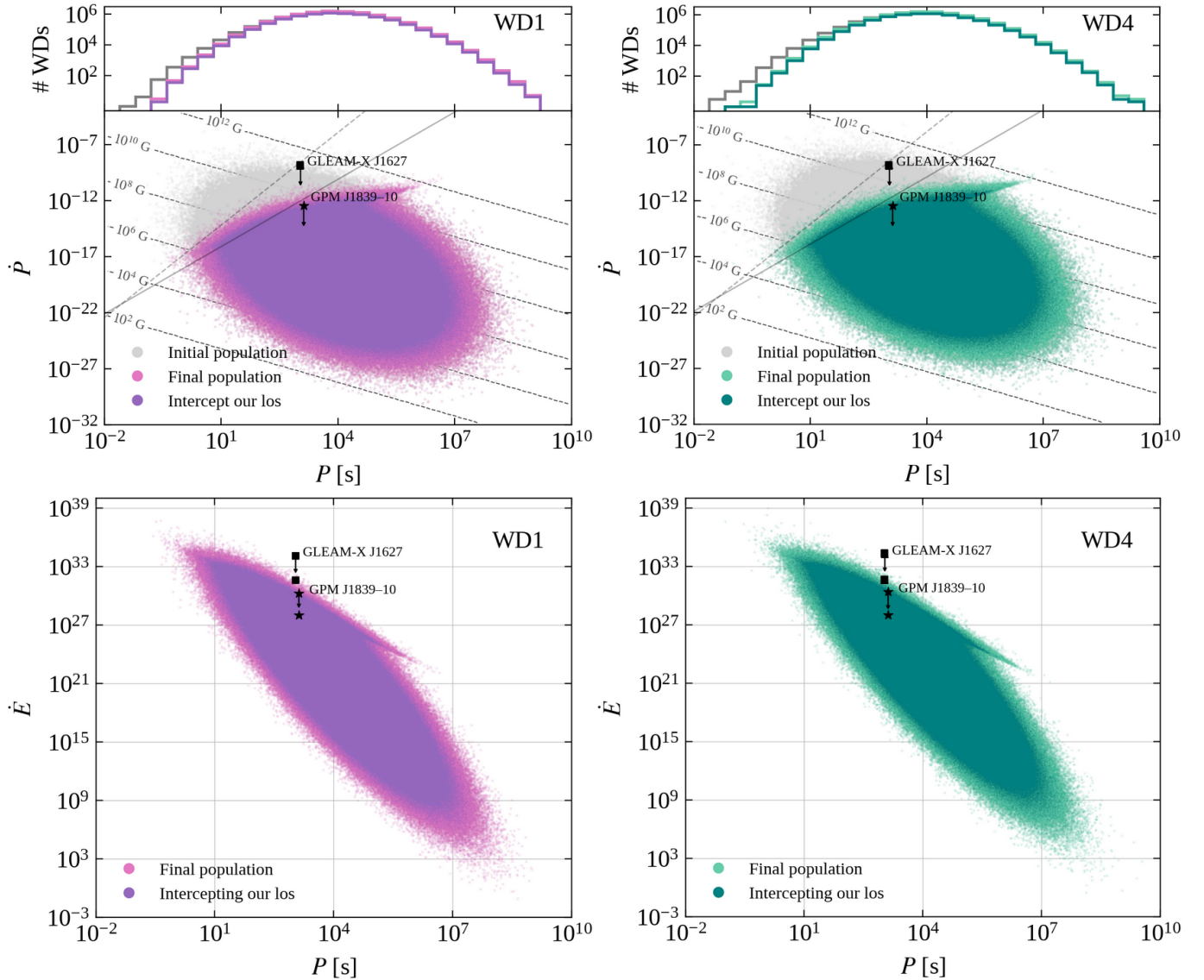


Figure 4. Population-synthesis results for models WD1 (purple) and WD4 (seagreen). Panels, lines and markers are similar to Fig. 2. Note that the death valley and the upper limits for the two long-period sources refer to the WD case (see Fig. 1, Secs. 2 and 3.2). Note that these two WD cases have different masses and radii, which is reflected in different B -field lines, death-valley and \dot{E} limits. Gray dots represent initial WD populations, pink and light seagreen final populations. The subsets of objects intercepting our line of sight are shown in purple and dark seagreen.

We simulate 10^7 NSs with random ages sampled from a uniform distribution up to a maximum age of 10^9 yrs. This translates to a birth rate of one NS per century, consistent with the Galactic core-collapse supernova rate (Rozwadowska et al. 2021). To assign each NS a birth field, we then sample the logarithm of the field (in Gauss) from a normal distribution with mean $\mu_{\log B} = 13.25$ and a standard deviation of $\sigma_{\log B} = 0.75$ (see, e.g., Gullón et al. 2014, 2015; Cieřlar et al. 2020). Unless stated otherwise, we adopt $M_{\text{NS}} = 1.4 M_{\odot}$ and $R_{\text{NS}} = 11$ km.

We sample the logarithm of the initial period from a normal distribution with mean $\mu_{\log P} = -0.6$ (corre-

sponding to 0.25 s) and standard deviation $\sigma_{\log P} = 0.3$ (Popov et al. 2010; Gullón et al. 2014; Xu et al. 2023). We further incorporate magnetic-field decay due to Ohmic dissipation and the Hall effect through magnetothermal evolution curves from Viganò et al. (2013b, 2021) and assume a radio beam angular aperture $\propto P^{-1/2}$ (Lorimer & Kramer 2012). Model NS1_Bdecay serves as a reference with standard population assumptions (Fig. 2 top-left). These are typical initial parameters compatible with the current observed pulsar population. However, they do not predict any long-period pulsars.

We continue with investigating more extreme scenarios, focusing first on zero field decay. Strong fields could be maintained over long timescales if electric currents are predominantly present in the NS core (e.g., [Viganò et al. 2021](#)). Consequently, NSs experience a more pronounced spin-down, reaching longer periods. For model `NS1_Bconst`, we thus repeat the set-up of `NS1_Bdecay` but with constant B -field at the very limit of what is physically viable. However, adding the constant- B assumption is insufficient to slow down the population substantially (see Tab. 1). For subsequent models, we continue with the extreme constant B -field case to explore the impact of other assumptions.

In model `NS2_Bconst`, we also relax the standard beaming assumption, adjusting the radio beam angular aperture to obtain a duty cycle of 20% in line with observations of GLEAM-X J1627–52 and GPM J1839–10. This results in an increase of the number of pulsars crossing our line of sight (see Fig. 2 top-right and bottom panels). For the remaining simulations, we thus maintain this prescription of the beaming unless stated otherwise.

Next, we explore different initial spin-period distributions, mimicking a possible interaction with initial fallback accretion (see, e.g., [Alpar et al. 2001](#); [Ertan et al. 2009](#); [Tong et al. 2016](#); [Ronchi et al. 2022](#)). For models `NS3_Bconst` to `NS6_Bconst`, we add a power law with an arbitrary cut-off at a period of 10^5 s to the aforementioned log-normal distribution of the observed pulsar population. We specifically consider a power law, as the spin-down is likely determined by different fallback accretion rates. Note that the cut-off does not affect our final results, but reflects the maximum spin reachable by fallback accretion: see Figs. 3–4 of [Ronchi et al. \(2022\)](#). We arbitrarily assume that both distributions are equally normalized, sampling 50% of NSs from either distribution, maintaining a birth rate of 1 NS per century. This prescription is still consistent with the log-normal population resulting in the observed radio pulsars ([Gullón et al. \(2015\)](#); see also yellow dots in Figs. 2 and 3). For models `NS3_Bconst` and `NS4_Bconst` (see Fig. 3 left panels), we assume a corresponding power-law index of -3 and -1, respectively. `NS5_Bconst` investigates a duty cycle of 10%, while for `NS6_Bconst`, we explore the effect of the assumed mass, setting $M_{\text{NS}} = 2M_{\odot}$.

Since stronger magnetic fields enhance the spin-down, we also investigate the effect of a bimodal B -field distribution (four models denoted with an asterisk (*) in Tab. 1). Besides the log-normal distribution, we consider that 50% of NSs are formed with a strong field uniformly distributed in $\log B \in [13.5, 14.5]$ following [Gullón et al. \(2015\)](#). `NS2*_Bdecay` and `NS2*_Bconst` consider only the

log-normal for the initial period distribution and a decaying and constant magnetic field, respectively, while for `NS4*_Bdecay` and `NS4*_Bconst`, we explore the log-normal plus power law for the initial period (see Fig. 3 right panels).

Using the same prescription as [Gullón et al. \(2014\)](#), we have checked that all population models presented here are consistent with the observed pulsar population. This is mainly due to the low rotational power and long periods of the resulting hidden pulsars.

3.2. WD population synthesis

MWDs spin down slower than NSs due to larger moments of inertia, larger spin periods and lower B -fields. Moreover, magnetic fields of MWDs do not exhibit relevant magnetic-field decay due to longer Ohmic dissipation timescales (e.g., [Cumming 2002](#)) and can be taken as constant ([Ferrario et al. 2020](#)). Consequently, current isolated WD periods and magnetic-fields strengths closely reflect those at birth.

To model these birth distributions, we consider a sample of 37 MWDs with reliable spin-period and magnetic-field measurements ([Ferrario et al. 2020](#)). We fit Gaussian functions to the distributions of the logarithm of the periods and B -fields, deriving a mean of $\mu_{\log P} = 3.94$ and standard deviation of $\sigma_{\log P} = 1.0$, and $\mu_{\log B} = 6.91$ and $\sigma_{\log B} = 1.09$, respectively. For our population synthesis, we then simulate 10^8 MWDs with ages drawn from a uniform distribution up to a maximum of 10^9 yr, consistent with a birth rate of 10 per century derived assuming a Galaxy radius of 20 kpc and 10% of the WD being magnetic (see, e.g., [Holberg et al. 2016](#) but also [Bagnulo & Landstreet 2021](#) who recently found 22%), and assign initial P and B values from our fitted distributions. Results of four simulation configurations are summarized in Tab. 1 and Fig. 4.

We further assume a WD radio beam angular aperture independent of P . For models `WD1` and `WD2`, we adjust our approach to obtain a 20% and 10% duty cycle, respectively. For `WD3` and `WD4`, we set the beaming as in `WD1` but vary mass and radius. In particular, using the Hamada-Salpeter mass-radius relation for He WDs ([Hamada & Salpeter 1961](#)), we consider $M_{\text{WD}} = 1.2 M_{\odot}$ and $R_{\text{WD}} = 4000$ km for a high-mass WD in `WD3` and $M_{\text{WD}} = 0.6 M_{\odot}$ with $R_{\text{WD}} = 9000$ km for a low-mass WD in `WD4`.

4. DISCUSSION AND CONCLUSION

Wide-field radio interferometers have begun to revolutionize our understanding of the transient radio sky. Until recently, coherent, polarized and periodic radio emission was characteristic of NS pulsars with periods $\lesssim 20$ s, a period range attributed to magnetic-field

Table 1. Population-synthesis results for isolated NSs and MWDs.

Model	Initial P	Beaming	Total $N/10^3$ [l.o.s.]			Total $N/10^3$ with $\dot{E} > 10^{27}$ erg s $^{-1}$ [l.o.s.]		
			$P = 10^{1-2}$ s	$P = 10^{2-3}$ s	$P = 10^{3-5}$ s	$P = 10^{1-2}$ s	$P = 10^{2-3}$ s	$P = 10^{3-5}$ s
NEUTRON STARS								
NS1_Bdecay	Log-N	pulsars	629.51 [9.22]	6.69 [0.02]	0.01 [0.00]	2.49 [0.05]	0.01 [0.00]	0.00 [0.00]
NS1_Bconst	Log-N	pulsars	4560.95 [31.15]	3357.42 [3.70]	574.38 [0.09]	2797.74 [24.68]	34.62 [0.06]	0.00 [0.00]
NS2_Bconst	Log-N	20%	4564.26 [1360.90]	3355.02 [799.39]	573.61 [120.38]	2799.49 [876.59]	34.70 [8.75]	0.00 [0.00]
NS3_Bconst	Log-N+PL(-3)	20%	4568.02 [1417.86]	3364.06 [818.03]	573.68 [122.11]	2799.46 [915.60]	34.78 [9.09]	0.00 [0.00]
NS4_Bconst	Log-N+PL(-1)	20%	3425.36 [1302.58]	3344.05 [1341.96]	2291.68 [1475.93]	1920.09 [706.18]	26.38 [8.52]	0.00 [0.00]
NS5_Bconst	Log-N+PL(-1)	10%	3425.41 [603.07]	3345.82 [646.41]	2289.66 [838.73]	1920.40 [320.11]	26.44 [3.62]	0.00 [0.00]
NS6_Bconst ^o	Log-N+PL(-1)	20%	3551.79 [1364.31]	3158.14 [1298.75]	2200.36 [1453.03]	2269.94 [837.21]	37.55 [12.22]	0.00 [0.00]
NS2_Bdecay [*]	Log-N	20%	827.50 [367.95]	3.37 [0.93]	0.00 [0.00]	3.75 [1.74]	0.00 [0.00]	0.00 [0.00]
NS2_Bconst [*]	Log-N	20%	2621.41 [765.23]	5849.46 [1342.22]	774.43 [168.48]	1656.60 [504.92]	77.12 [19.16]	0.00 [0.00]
NS4_Bdecay [*]	Log-N+PL(-1)	20%	1511.96 [977.49]	895.09 [665.54]	1786.98 [1330.37]	3.92 [2.27]	0.01 [0.00]	0.00 [0.00]
NS4_Bconst [*]	Log-N+PL(-1)	20%	1942.87 [717.60]	5077.88 [1733.97]	2508.41 [1565.64]	1136.06 [406.37]	58.33 [18.82]	0.00 [0.00]
WHITE DWARFS								
WD1	Log-N	20%	1929.55 [1406.56]	14485.85 [10649.08]	69050.05 [51234.73]	1823.72 [1328.54]	7956.49 [5803.80]	3880.60 [2729.91]
WD2	Log-N	10%	1928.76 [817.16]	14484.90 [6225.08]	69042.10 [30034.14]	1822.90 [771.63]	7955.59 [3386.88]	3883.30 [1577.85]
WD3 ^o	Log-N	20%	2147.21 [1576.08]	14705.23 [10871.34]	68592.09 [51016.48]	1894.94 [1389.56]	5687.17 [4172.56]	1664.71 [1176.52]
WD4 ^o	Log-N	20%	1579.74 [1141.63]	13837.27 [10076.93]	70003.37 [51617.09]	1542.90 [1114.49]	9672.34 [6989.46]	7872.76 [5454.37]

NOTE—All models were evolved for 10^9 yr assuming a birth rate of 1 NS and 10 MWD per century. Unless specified otherwise, NSs have $1.4M_{\odot}$ and 11 km radii, while MWDs have $1M_{\odot}$ and 6000 km radii. Numbers in parentheses denote the assumed PL slope. Numbers in brackets are the sub-sample of simulated neutron stars that cross our line of sight [l.o.s.] for their respective beaming. Note that all reported numbers are in units of 10^3 , hence being integers.

* Bimodal magnetic field distribution (see text).

^o NS6_Bconst assumes a $2M_{\odot}$ NS mass, WD3 a mass of $1.2M_{\odot}$ and 4000 km radius, and WD4 a mass of $0.6M_{\odot}$ and 9000 km radius.

decay and a resistive crust (Pons et al. 2013). However, in the last year, two ultra-long period systems, GLEAM-X J1627–52 and GPM J1839–10 (Hurley-Walker et al. 2022, 2023), and the slow pulsar PSR J0901-4046 (Caleb et al. 2022) were discovered.

In this work, we study long-period pulsars in the rotating NS and WD dipole scenario, one of the most likely interpretations given their coherent and highly polarized emission, and perform population synthesis.

1. While the classical scenario for NS pulsar radio emission based on magnetospheric pair production can in principle accommodate GLEAM-X J1627–52, it cannot account for GPM J1839–10 as the source sits below even the most extreme death line (Fig. 1). However, note that both objects have radio luminosities exceeding their \dot{E} s by 2-3 orders of magnitudes (Hurley-Walker et al. 2023). Hence, the emission scenario is necessarily more complex than for normal radio pulsars (possibly resembling radio magnetars; see Fig. 6 in Rea et al. 2022).

2. Figure 1 also highlights that a similar mechanism in MWDs could in principle contribute to the radio emission of GLEAM-X J1627–52, AR Sco and J1912–4410. However, GPM J1839–10’s bright radio emission cannot be easily reconciled even in the isolated MWD case. Note that interactions with a companion’s wind can enhance the radio emission (as for AR Sco and J1912–4410; see also Geng et al. 2016). For GLEAM-X J1627–52 optical and IR observations could rule out main sequence companion stars (Rea et al. 2022), but for GPM J1839–10

a similar constrain was not possible given the larger distance (Hurley-Walker et al. 2023).

3. Our NS population synthesis models (Tab. 1) show that a large population of long-period radio emitters cannot be easily explained as NS pulsars. Neither standard population assumptions nor the most extreme scenarios invoking zero field decay (Fig. 2), initial slow-down via fallback accretion, 20% duty cycles or stronger birth fields (Fig. 3) result in sufficiently energetic NS pulsars with periods > 1000 s pointing towards the Earth (irrespective of mass). A difference by a factor of a few in the NS birth rate does not alter this conclusion.

4. On the other hand, WD population synthesis highlights that long-period MWD are more common than NS pulsars, with lower masses and larger radii leading to enhanced spin down and more slow rotators (Tab. 1). However, Fig. 1 shows that the known sample of isolated MWDs are not expected to emit coherent radio emission via standard pair production, being all below the most extreme death line.

In conclusion, the classical particle acceleration mechanism for rotating dipoles fails to provide a satisfactory explanation for the radio emission of GPM J1839–10 in either the NS or WD scenario. In contrast, all observed isolated MWDs with measured B -fields fall below the most extreme death lines, possibly explaining their radio non-detection. The radio emission observed from the binary WDs AR Sco and J1912–4410 might be enhanced by the presence of their compan-

ion star within the WD pulsar lightcylinder. Deep optical and IR observations ruled out main sequence stars for GLEAM-X J1627–52 (Rea et al. 2022), but deeper observations are needed to exclude any binarity. On the other hand, GPM J1839–10’s limits (Hurley-Walker et al. 2023) cannot provide strong constraints given its larger distance.

Moreover, in the NS scenario, we do not expect a large population of ultra-long period pulsars under any (physically motivated or extreme) assumptions. While many more slow WD pulsars might be expected, however we still lack a mechanism to explain the bright radio emission. Therefore, if GLEAM-X J1627–52 and GPM J1839–10 are confirmed as isolated NS or WD pulsars, this would call for a revision of our understanding of radio emission from dipolar magnetospheres. Corroborating the NS scenario would further require a significant reexamination of our understanding of initial

NS parameters (birth rates, magnetic-field distribution, etc.) at the population level.

N.R., C.P.A., M.R., V.G. and F.C.Z. are supported by the ERC via the Consolidator Grant “MAGNESIA” (No. 817661), and by the program Unidad de Excelencia María de Maeztu CEX2020-001058-M. We acknowledge partial support from grant SGR2021-01269 (PI: Graber). C.P.A. and M.R.’s work has been carried out within the framework of the doctoral program in Physics of the Universitat Autònoma de Barcelona. N.H.W. is the recipient of an ARC Future Fellowship (No. FT190100231). F.C.Z. is also supported by a Ramón y Cajal Fellowship (RYC2021-030888-I). Dd.M. acknowledges financial support from ASI and INAF. We would like to thank A. Kawka, J. Isern, A. Harding, R. Turolla, D. Viganó and J. A. Pons for discussions. We also acknowledge the anonymous referee for the useful comments and suggestions that improved the manuscript.

REFERENCES

- Alpar, M. A., Ankay, A., & Yazgan, E. 2001, *ApJL*, 557, L61
- Bagnulo, S., & Landstreet, J. D. 2021, *MNRAS*, 507, 5902
- Bhattacharya, D., & van den Heuvel, E. P. J. 1991, *PhR*, 203, 1
- Buckley, D. A. H., Meintjes, P. J., Potter, S. B., Marsh, T. R., & Gänsicke, B. T. 2017, *Nature Astronomy*, 1, 0029
- Caiazzo, I., Burdge, K. B., Fuller, J., et al. 2021, *Nature*, 595, 39
- Caleb, M., Heywood, I., Rajwade, K., et al. 2022, *Nature Astronomy*, 6, 828
- Chatterjee, P., Hernquist, L., & Narayan, R. 2000, *ApJ*, 534, 373
- Chen, K., & Ruderman, M. 1993, *ApJ*, 402, 264
- Cieślak, M., Bulik, T., & Osłowski, S. 2020, *MNRAS*, 492, 4043
- Coti Zelati, F., Rea, N., Pons, J. A., Campana, S., & Esposito, P. 2018, *MNRAS*, 474, 961
- Cumming, A. 2002, *MNRAS*, 333, 589
- D’Ài, A., Evans, P. A., Burrows, D. N., et al. 2016, *MNRAS*, 463, 2394
- De Luca, A., Caraveo, P. A., Mereghetti, S., Tiengo, A., & Bignami, G. F. 2006, *Science*, 313, 814
- du Plessis, L., Wadiasingh, Z., Venter, C., & Harding, A. K. 2019, *ApJ*, 887, 44
- Ertan, Ü., Ekşi, K. Y., Erkut, M. H., & Alpar, M. A. 2009, *ApJ*, 702, 1309
- Ferrario, L., de Martino, D., & Gänsicke, B. T. 2015, *SSRv*, 191, 111
- Ferrario, L., Wickramasinghe, D., & Kawka, A. 2020, *Advances in Space Research*, 66, 1025
- Ferrario, L., & Wickramasinghe, D. T. 2005, *MNRAS*, 356, 615
- Geng, J.-J., Zhang, B., & Huang, Y.-F. 2016, *ApJL*, 831, L10
- Gullón, M., Miralles, J. A., Viganò, D., & Pons, J. A. 2014, *MNRAS*, 443, 1891
- Gullón, M., Pons, J. A., Miralles, J. A., et al. 2015, *MNRAS*, 454, 615
- Hamada, T., & Salpeter, E. E. 1961, *ApJ*, 134, 683
- Holberg, J. B., Oswalt, T. D., Sion, E. M., & McCook, G. P. 2016, *MNRAS*, 462, 2295
- Hurley-Walker, N., Rea, N., McSweeney, S. J., & et, A. 2023, *Nature*, ?, ?
- Hurley-Walker, N., Zhang, X., Bahramian, A., et al. 2022, *Nature*, 601, 526
- Lorimer, D. R., & Kramer, M. 2012, *Handbook of Pulsar Astronomy* (Cambridge University Press)
- Manchester, R. N., Hobbs, G. B., Teoh, A., & Hobbs, M. 2005a, *AJ*, 129, 1993
- . 2005b, *AJ*, 129, 1993
- Marsh, T. R., Gänsicke, B. T., Hümmelich, S., et al. 2016, *Nature*, 537, 374
- Olausen, S. A., & Kaspi, V. M. 2014, *ApJS*, 212, 6
- Pelicoli, I., Marsh, T. R., Buckley, D. A. H., et al. 2023, *Nature Astronomy*, arXiv:2306.09272
- Pelicoli, I., Sahu, S., Lyutikov, M., et al. 2024, *MNRAS*, 527, 3826

- Philippov, A., Tchekhovskoy, A., & Li, J. G. 2014, *MNRAS*, 441, 1879
- Pons, J. A., Viganò, D., & Rea, N. 2013, *Nature Physics*, 9, 431
- Popov, S. B., Pons, J. A., Miralles, J. A., Boldin, P. A., & Posselt, B. 2010, *MNRAS*, 401, 2675
- Rea, N., Borghese, A., Esposito, P., et al. 2016, *ApJL*, 828, L13
- Rea, N., Coti Zelati, F., Dehman, C., et al. 2022, *ApJ*, 940, 72
- Ronchi, M., Graber, V., Garcia-Garcia, A., Rea, N., & Pons, J. A. 2021, *ApJ*, 916, 100
- Ronchi, M., Rea, N., Graber, V., & Hurley-Walker, N. 2022, *ApJ*, 934, 184
- Rozwadowska, K., Vissani, F., & Cappellaro, E. 2021, *NewA*, 83, 101498
- Ruderman, M. A., & Sutherland, P. G. 1975, *ApJ*, 196, 51
- Spitkovsky, A. 2006, *ApJL*, 648, L51
- Suvorov, A. G., & Melatos, A. 2023, *MNRAS*, 520, 1590
- Tan, C. M., Bassa, C. G., Cooper, S., et al. 2018, *ApJ*, 866, 54
- Tauris, T. M. 2012, *Science*, 335, 561
- Tong, H., Wang, W., Liu, X. W., & Xu, R. X. 2016, *ApJ*, 833, 265
- Viganò, D., Garcia-Garcia, A., Pons, J. A., Dehman, C., & Graber, V. 2021, *Computer Physics Communications*, 265, 108001
- Viganò, D., Rea, N., Pons, J. A., et al. 2013a, *MNRAS*, 434, 123
- . 2013b, *MNRAS*, 434, 123
- Xu, K., Yang, H.-R., Mao, Y.-H., et al. 2023, *ApJ*, 947, 76
- Zhang, B., & Gil, J. 2005, *ApJL*, 631, L143
- Zhang, B., Harding, A. K., & Muslimov, A. G. 2000, *ApJL*, 531, L135